Rueda-García, L.; Bonet Senach, JL.; Miguel Sosa, P.; Fernández Prada, MÁ. (2021). Experimental analysis of the shear strength of composite concrete beams without web reinforcement. Engineering Structures. 229:1-17. https://doi.org/10.1016/j.engstruct.2020.111664

Experimental analysis of the shear strength of composite concrete beams without web reinforcement

Lisbel Rueda García, lisruega@cam.upv.es

José Luis Bonet Senach, jlbonet@cst.upv.es

Pedro Fco. Miguel Sosa, pmiguel@cst.upv.es

Miguel Ángel Fernández Prada, mafernan@cst.upv.es

Universitat Politècnica de València, Camí de Vera s/n, 46022 Valencia, Spain

Abstract

Composite concrete members without web reinforcement are often used in precast construction. The contribution of the cast-in-place concrete topping slab to vertical shear strength has been traditionally disregarded. However, significant cost savings can result from designing and assessing these structures if this contribution is considered. This paper presents the experimental study of a series of 21 monolithic and composite (precast beam and cast-in-place slab) specimens without web reinforcement, and with rectangular and T-shaped cross-sections, failing in shear. The vertical shear strength was analysed by the following test variables: cross-section shape, the existence of an interface between different aged concretes, strengths of the two concretes and the differential shrinkage effect. From these experimental tests, it was concluded that the slab contributed to shear strength, the use of high-strength concrete slightly increased specimens' shear strength and the differential shrinkage did not reduce shear strength. Specimens' failure modes were analysed based on their shear transfer mechanisms, noticing that the arching action in the slab was considerable after critical shear crack formation. The vertical shear strength experimental results were well predicted by the codes' formulations (Eurocode 2, Model Code 2010 and ACI 318-19) when composite beam depth was taken for the calculations instead of beam depth. Codes significantly underestimated the horizontal shear strengths of the composite specimens.

Keywords: reinforced concrete, composite beam, T-shaped beam, precast construction, vertical shear strength, horizontal shear strength, differential shrinkage.

Highlights

- Shear in monolithic and composite concrete beams without stirrups was studied
- Slab width, interface, concrete strength and differential shrinkage were analysed
- The interface between concretes modified the critical shear crack direction
- The slab contributed to increase the shear strength of the composite specimen
- An over-strength of the T-shaped composite beams due to arching action was noted

Nomenclature

a	shear span
b	concrete section width
C	compression force at the slab
c	concrete cover
c_a	coefficient for the adhesive bond
d	effective depth
d_g	maximum size of the aggregate
E_c	modulus of elasticity of concrete
E_s	modulus of elasticity of reinforcement
f_c	compressive strength of the concrete measured in cylinder
$f_{c,28}$	compressive strength of the concrete measured in cylinder at the age of 28 days
$f_{c,min}$	minimum compressive strength of the two concretes of the composite beam
$f_{c,wa}$	weighted average of the beam's and slab's concrete compressive strengths estimated from the area ratio
f_{ct}	tensile strength of concrete
f_u	tensile strength of reinforcement
f_y	yield strength of reinforcement

h	overall height of member
M_{Ed}	design value of the applied bending moment
V_{Ed}	design shear force in the section considered
$V_{R,code}$	shear strength predicted by the design code
$V_{R,max1}$	experimental first local maximum of the shear-deflection relation
$V_{R,max2}$	experimental second local maximum of the shear-deflection relation
x	distance between a beam's instrumented cross-sections
z	internal lever arm
γ_c	partial safety factor for concrete material properties
γ_s	partial safety factor for steel material properties
ε_u	reinforcement strain at maximum load
ε_x	longitudinal strain at the mid-depth of the effective shear depth at the control section
ρ_l	reinforcement ratio of tension longitudinal reinforcement
σ_n	the lowest expected compressive stress resulting from an eventual normal force acting on the interface
$\tau_{R,code}$	horizontal shear stress predicted by the design code
$\tau_{R,exp}$	average experimental horizontal shear stress
$\varnothing$	nominal diameter of a reinforcing bar

1. Introduction

Cast-in-place concrete is frequently used in precast concrete construction to integrate structural elements. Precast concrete beams, together with cast-in-place concrete over them, form what is commonly known as a composite concrete beam. This type of construction has been widely used for decades and its employment is still growing. Given the many existing constructions involving this construction system, ranging from structural floors to concrete beams bridges, studying their structural behaviour is especially relevant. In particular, the study of composite reinforced concrete beams

without shear reinforcement is important because of its applicability to building construction [1].

Traditionally, research on composite beams has focused on their horizontal shear strength [2] given the critical importance of adherence between concretes so that composite beams appropriately behave. Among these studies, Loov and Patnaik [3], Kovach and Naito [4] or Fang *et al*. [5] analysed the effect of interface roughness, the shear span-depth ratio, properties of concretes and shear reinforcement. One of the conclusions was that the current codes, especially ACI 318-19 [6], underestimate the horizontal shear strength of the composite beams' interface between concretes, almost always requiring the presence of interface reinforcement.

In the last century, vertical shear strength in monolithic beams has been widely studied, but no agreement about structural shear design has yet been reached between the existent codes, which provide semi-empirical expressions to evaluate the shear strength of concrete beams that are excessively scattered [7]. Nonetheless, the determination of composite beams' resistance to vertical shear solicitations has not been studied in-depth [2]. Indeed, in both the design and assessment of composite beams' shear strength, the contribution of the slab to shear strength is commonly omitted to stay on the safety side. This omission seems reasonable because shear strength is a phenomenon that still involves many unknowns. However, that contribution does exist and, therefore, it should be considered in calculations for economical designs [2]. In the scientific literature, some publications on the experimental analysis of full-scale composite concrete beams can be found [8,9]. They show their structural behaviour, focusing analyses on verifying their shear strength according to design codes. However, no studies have analysed the contribution of the cast-in-place slab to the composite beam's shear strength.

Regarding the different codes' vertical shear strength considerations in composite beams, some codes, like MC-10 [10], do not refer to such elements. Other codes, like EC2 [11] (Section 10.9.3(8)) and ACI 318-19 [6] (Section 22.5.4), allow the possibility of considering the whole composite beam to resist shear as long as the horizontal shear at the interface between the two concretes is verified. Only ACI 318-19 [6] specifies how this composite beams can be calculated: using the properties of the individual elements or the properties of the element that result in the most critical value.

Nowadays, it is well-known that the existence of an interface between two concretes varies the pattern of shear cracks in relation to monolithic beams [2,12,13]. Notwithstanding, Halicka [14] revealed that few experimental tests done with composite

concrete beams subjected to vertical shear actually consider the influence of interface cracking on the composite element's vertical shear behaviour. In fact the latest studies in composite beams [2] have neither analysed the influence of the interface on vertical shear strength nor compared this behaviour to that of monolithic beams.

Recently, Kim *et al*. [2,12] carried out an experimental programme of the vertical shear strength of rectangular composite beams made of normal-strength concrete and high-strength concrete in beams with and without web reinforcement. Regarding the beams without web reinforcement [2], they observed that the use of high-strength concrete on the precast beam did not significantly increase the shear strength of the composite element, that a greater longitudinal reinforcement ratio increased the shear strength of the beams, and that the shear strength decreased with increasing the shear span-effective depth ratio. Kim *et al.* [2] evaluated the shear strength of the composite elements using the average concrete strength obtained from the area ratio of the two concretes used in the cross-section, and observed that current design codes safely estimated the shear strength of the composite beams. They remarked that the total number of existent experimental tests that analyse composite beams' shear strength is still insufficient. The shape of beams and other parameters need to be considered. Consequently, the development of new shear strength evaluation models for composite beams is limited.

Extending studies to new cross-sectional shapes is important because the behaviour of the structural elements compound of a precast beam with a cast-in-place slab on top could resemble in that of a composite T-shaped beam in some cases. Examples of actual structural elements with this cross-sectional shape and without web reinforcement are shown in Fig. 1. Furthermore, the inclination and shape of critical shear cracks vary when section width undergoes abrupt variations [15,16]. It has also been long since known [17] that T-shaped beams fail in shear instead of bending in a wider range of shear span-effective depth ratios (*a/d*). All this proves the importance of studying shear in T-shaped composite elements.

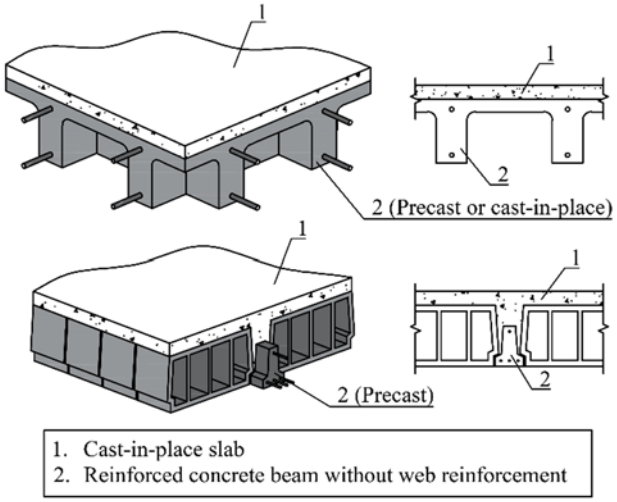

Fig. 1. Examples of structural elements compound of a reinforced concrete beam without web reinforcement and a cast-in-place slab.

The present research work intends to study the contribution of the cast-in-place slab's depth and width to the vertical shear strength in composite reinforced concrete beams without web reinforcement. This objective is experimentally studied in rectangular and T-shaped monolithic and composite beams by analysing the effect of the cross-section shape, the existence of an interface between two different aged concretes, the strengths of the two concretes and the effect of differential shrinkage between concretes. Moreover, the shear transfer mechanisms developed in the more relevant loading stages while running tests are analysed. The validity of the current design methods is also studied.

This research work is especially significant in the precast construction field as it intends to increase the number of existent experimental tests, and contribute with them to the extension of current codes with a more economical perspective when both designing new construction and assessing existent structures.

2. Test programme

2.1. Test parameters

Twenty-one experimental tests were designed to analyse the influence of the following four variables on the shear strength of composite reinforced concrete beams without web reinforcement:

- The cross-sectional shape (Fig. 2). It was firstly considered a reference rectangular section type A that equals that of the precast beams used in composite specimens. Secondly, three different sections with the same depth

and web width, but with different flange widths, were adopted: section B, without flanges; section C with flange width that equals slab depth, which is frequently assumed in the literature [1,15]; section D, whose flange width was twice the slab depth.

- The existence of an interface between two different aged concretes. Specimens A1, B1 and C1 were fabricated with one concrete (monolithic beams) and specimens B2, C2 and D2 with two concretes (composite beams).
- The strengths of the two concretes of the composite beam. Two types of concretes were used: normal-strength concrete (NSC), with a nominal compressive strength of 30 MPa; and high-strength concrete (HSC), with a nominal compressive strength of 60 MPa. NSC represented a concrete commonly used in cast-in-place elements, while HSC was representative of a concrete usually poured for fabricating precast beams.
- The differential shrinkage between concretes. In a composite structure, differential shrinkage is a loading case itself, since it generates shrinkage stresses in the structure that are mainly compressive in the base layer and tensile in the overlay, as Silfwerbrand stated [18]. In 10 of the 12 composite specimens, the slab's concrete was poured 24 h after the beam's concrete. This way, the construction process was faster and the differential shrinkage between the beam's and the slab's concretes was reduced. This fabrication timeline was already carried out in previous experimental studies on vertical and horizontal shear strength of composite beams [2–4,12]. However, the described tests reflect the difference between concrete classes at the beam and the slab, but not the influence of different aged concretes at the beam and the slab. Hence, in order to analyse if different ages between concretes had a significant influence on vertical shear strength in this experimental programme, the fabrication process was modified in two of the specimens, where the slab's concrete was poured when the beam's concrete shrinkage had stabilised.

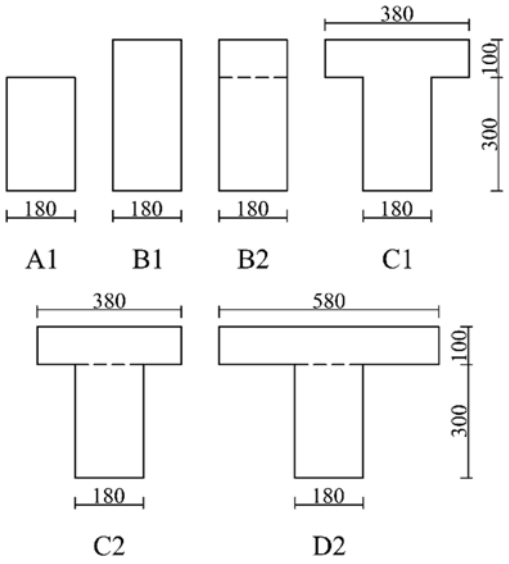

Fig. 2. Cross-section types (dimensions in mm).

The number of specimens of each series is shown in Table 1. Specimens were named using the notation *xOPyzk(j)*, where:

- "*xO*" denoted the series of beams without web reinforcement: NO for the specimens in which the beam's concrete was NSC, HO for specimens in which the beam's concrete was HSC, and DO for the beams fabricated with differential shrinkage between concretes.
- "*Py*" for the fabrication batch (from P1 to P5 as the beams fabrication process of pouring beam's and slab's concretes was conducted 5 times).
- "*z*" denoted the cross-sectional shape (A, B, C, or D) (Fig. 2).
- "*k*" denoted the number of different concretes used to fabricate the specimen (1 for monolithic beams, 2 for composite beams).
- "*j*" was used only when more than one specimen was fabricated with identical previous characteristics ("a" or "b").

Table 1. Characteristics of beams' series.

Series	Type of beam's concrete	Type of slab's concrete	Number of specimens for each cross-sectional type					
			A1	B1	B2	C1	C2	D2
NO	NSC	NSC	2	2	3	2	2	2
HO	HSC	NSC	1	1	1	1	1	1
DO	NSC	NSC	0	0	2	0	0	0

The fixed parameters in all the beams were: longitudinal reinforcement ratio (ρ_l = 4.0%), shear span-effective depth ratio (a/d = 4.0), relative concrete cover (c/h = 0.16) and interface roughness (very rough interface). Longitudinal reinforcement was designed to avoid bending failure. The shear span-effective depth ratio was fixed in

order to foster a shear failure in both the rectangular and T-shaped beams based on the observations of Kani's valley [17]. Concrete cover and spacing between rebars were chosen according to the code provisions. A very rough interface treatment was used between concretes based on the conclusions of a previous study carried out by the authors [19]. According to the classification of failure mechanisms of composite concrete beams shown in Halicka [14], horizontal shear failure occurs when interface cracking appears prior to diagonal cracking. In Rueda-García *et al.* [19], beams with the same characteristics as those of this research work presented interface cracking after the diagonal cracking, thus proving the effectiveness of the given interface treatment for not failing in horizontal shear nor showing a monolithic behaviour. The interface reinforcement turned out to be unnecessary, even though the code calculations predicted horizontal shear failure.

Beam and slab were fabricated on the same formwork, without lifting the beam after the first concrete pouring. Thus in this experimental study, both the beam and slab were simultaneously loaded.

2.2. Test specimens

All the specimens' dimensions and reinforcements are specified in Fig. 3. Specimens type B, C and D had a total length of 3.50 m (2.74 m between supports). Two-point non-centred vertical loading was applied, with a 0.40-metre space between loads, to obtain a weak 1.34-metre shear span without shear reinforcement in which failure was expected. The other 1.00-metre span was reinforced to avoid its shear failure and induce the failure at the 1.34-metre span. Specimens type A were 3.16 m long (2.40 m between supports) to obtain the fixed shear span-effective depth ratio value (a/d = 4.0).

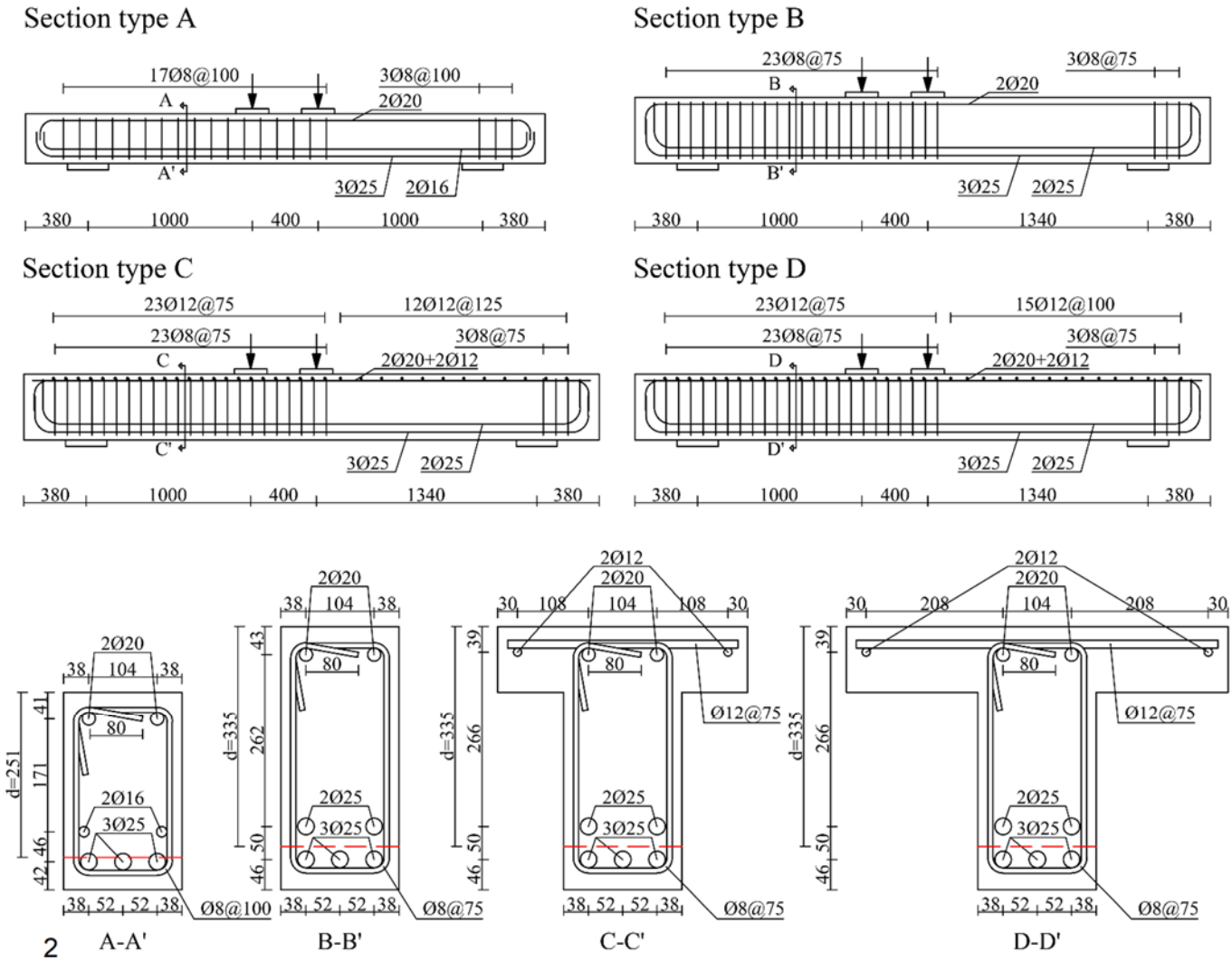

Fig. 3. Dimensions and reinforcement of beams with section types A, B, C and D (dimensions in mm).

Some of these beams were composite beams with two layers of different aged concretes. The first layer, 0.30 m high, represented the precast beam of the composite beam. The second layer, 0.10 m high, was cast on the previous one and represented the cast-in-place concrete slab.

2.3. Fabrication of specimens

Concrete casting was done by dividing the 21 specimens into five fabrication batches (P1 to P5 in Table 2) to eliminate the variable concrete strength when comparing the test results of the specimens in the same batch. In series NO and HO, concrete casting was performed in two phases. In the first phase, the beam's concrete was poured and the surface was raked before concrete hardened to obtain a very rough interface with dents of approximately 6 mm deep (from peak to valley) and a maximum spacing of 40 mm between peaks (dimensions defined in current design codes [6,10,11]). An example of this roughness is shown in Fig. 4. In the second phase done 24 h later, the

slab's concrete was poured over the beam's concrete. Concrete was cured for 7 days before moving away the formworks.

Table 2. Summary of the test results.

Series	Fabri-cation batch	Specimen	$f_{c,28}$ beam (MPa)	$f_{c,28}$ slab (MPa)	f_c beam (MPa)	f_c slab (MPa)	E_c beam (MPa)	E_c slab (MPa)	f_{ct} beam (MPa)	f_{ct} slab (MPa)	$V_{R,max1}$ (kN)	$V_{R,max2}$ (kN)	$\tau_{R,exp}$ (MPa)	Cracking mode (*)
NO	P1	NOP1B2	32	31	32	31	35228	31848	2.41	2.72	91	(**)	1.48	DC+HC
	P2	NOP2A1	36	33	39	-	32294	-	1.86	-	75	84	-	DC
		NOP2B1			40	-	31507	-	2.39	-	88	62	-	DC
		NOP2C1			40	-	31507	-	2.39	-	72	90	-	DC+HC
		NOP2C2			39	34	34732	25789	2.29	2.77	94	83	2.59	DC+HC
		NOP2D2			39	34	34732	25789	2.29	2.77	84	80	1.99	DC+HC
	P3	NOP3A1	30	37	33	-	25329	-	2.93	-	62	72	-	DC
		NOP3B1			30	-	28717	-	2.41	-	81	57	-	DC
		NOP3B2a			31	38	26604	29635	2.45	1.77	70	41	-	DC
		NOP3B2b			31	38	26604	29635	2.45	1.77	86	92	2.04	DC+HC
		NOP3C1			30	-	28717	-	2.41	-	79	83	-	DC+HC
		NOP3C2			29	38	28403	32502	2.37	3.02	86	79	1.90	DC+HC
		NOP3D2			29	38	28403	32502	2.37	3.02	85	130	(***)	DC+HC
HO	P4	HOP4A1	61	31	61	-	36655	-	3.29	-	86	81	-	DC
		HOP4B1			63	-	36492	-	3.34	-	93	67	-	DC
		HOP4B2			63	31	36655	29521	3.70	2.36	101	71	-	DC
		HOP4C1			63	-	36492	-	3.34	-	90	88	-	DC+HC
		HOP4C2			63	31	36655	29521	3.70	2.36	86	97	2.01	DC+HC
		HOP4D2			63	31	36655	29521	3.70	2.36	99	116	1.54	DC+HC
DO	P5	DOP5B2a	24	36	29	37	24939	31243	2.44	2.82	88	72	2.04	DC+HC
		DOP5B2b			29	37	24939	31243	2.44	2.82	89	97	1.91	DC+HC

(*) Cracking mode at $V_{R,max1}$: DC is diagonal cracking; HC is horizontal cracking (at the interface in composite beams or at the plane in which the section width changes in T-shaped beams).
(**) Loading process was finished after first load drop.
(***) Calculation was not possible due to gauges failure.

In series DO, concrete shrinkage was measured after pouring the beam's concrete and raking the surface. After 134 days when the data revealed that concrete shrinkage had stabilised, the slab's concrete was poured.

Fig. 4. Very rough interface conditions.

2.4. Material properties

The properties of concrete were measured according to UNE-EN 12390 [20–22] and were calculated as the average of two tested concrete cylinders (300 mm high, 150 mm diameter) at the age of 28 days and each day a specimen was tested. Specimens were tested approximately 30 days after being fabricated. The compressive strength range of concrete at the testing age was between 29 and 40 MPa for NSC, and between 61 and 63 MPa for HSC. The modulus of elasticity of concretes varied from 25 to 35 GPa for NSCs and from 36 to 37 GPa for HSC. The tensile strength of concretes varied from 1.77 to 3.02 MPa for NSCs and from 3.29 to 3.70 MPa for HSC. Table 2 shows the nominal compressive strengths f_c of both the beam's and slab's concretes measured for each specimen the day it was tested and at the age of 28 days ($f_{c,28}$). The moduli of elasticity E_c and the tensile concrete strength f_{ct} measured the day the specimen was tested are also shown in Table 2.

For NSCs, the amount of Portland cement, the water-cement ratio and the maximum aggregate size (d_g) were 325 kg/m^3, 0.52 and 10 mm, respectively. For HSC, these same properties were 500 kg/m^3, 0.44 and 10 mm, respectively.

The steel type used for reinforcement was C class (according to EC2 [11]). Table 3 offers the results of the characterisation tests carried out according to UNE-EN ISO 6892 [23]. To determine the average values of the steel mechanical properties, two pieces of reinforcing steel were tested for each nominal diameter.

Table 3. Average values of the flexural and transversal reinforcement properties.

Series	NOP1			NOP2, NOP3, HOP4, DOP5				
Ø (mm)	8	20	25	8	12	16	20	25
f_y (MPa)	534	534	556	538	533	561	585	557
E_s (GPa)	189	206	197	203	207	240	192	199
f_u (MPa)	662	639	670	658	638	675	673	666
ε_u (%)	10.1	10.5	9.7	12.0	13.3	31.9	41.0	48.3

2.5. Instrumentation

Three 1000 kN load cells were used to take continuous measurements of the force in the hydraulic jack and the reactions at the bearing points.

As shown in Fig. 5a, lineal variable displacement transformers (LVDTs) were used to measure the displacements on the concrete surface. Five vertical LVDTs (V1 to V5) were placed at the supports and below three beam sections to measure vertical displacements. Four horizontal LVDTs (H1 to H4) were used to record the possible slips between the slab and beam along the interface, to analyse the influence of the interface in the behaviour of the specimen under vertical shear. Two vertical LVDTs (O1 and O2) were connected to the upper and bottom parts of two cross-sections to detect the beginning of the crack opening of either the web or the interface.

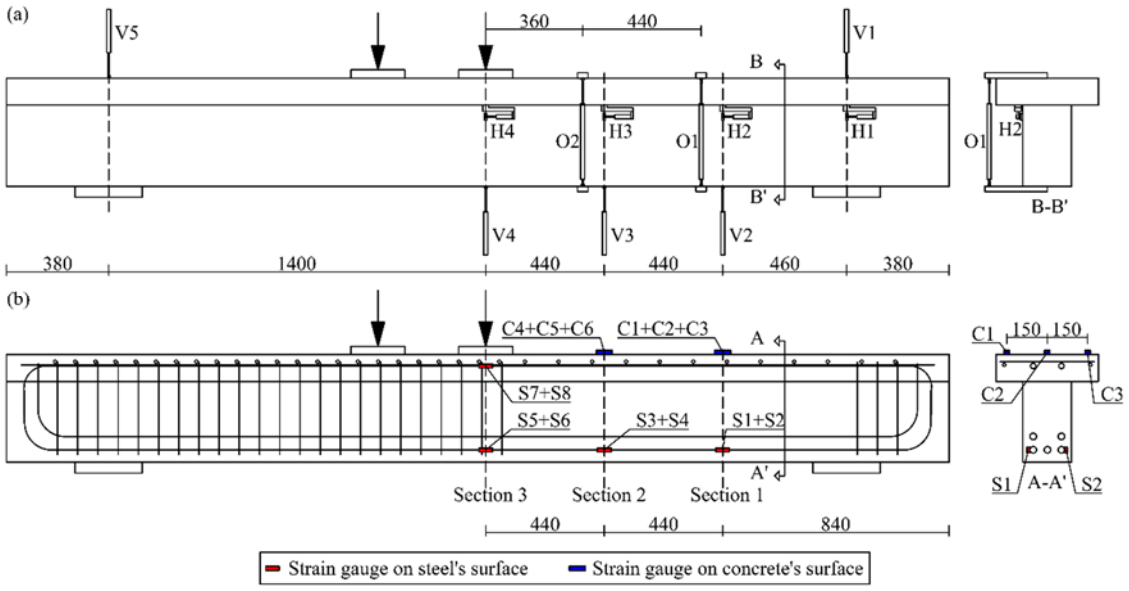

Fig. 5. Instrumentation for the shear test of a beam with section type C: (a) LVDTs; (b) strain gauges (dimensions in mm).

As shown in Fig. 5b, six strain gauges of 120 Ω resistance and 2 mm measuring length (S1 to S6) were used to measure the strains of the tension longitudinal reinforcement steel in three sections (Sections 1, 2 and 3). A pair of strain gauges (S7 and S8) was also placed on the compression longitudinal reinforcement below the central point load.

Strain gauges of 120 Ω resistance and 60 mm measuring length were used to measure the strains on the concrete surface. Two (in rectangular beams) or three (in T-shaped beams) strain gauges were placed on top of the concrete slab in two sections (C1 to C6 in Fig. 5b). The distance between strain gauges on the concrete surface was 100 mm in beams with section type B, 150 mm in section type C and 250 mm in section type D.

While testing, two digital cameras took pictures of the principal span at a rate of 0.5 Hz. A high-speed camera was used to record brittle failures and to detect the beginning of failure.

Additionally, the shrinkage of the two beams of series DO was monitored for almost 4 months starting from day 2 after pouring concrete. Different techniques were used: continuous measurements of two LVDTs placed horizontally to each beam's end (H1 and H2 in Fig. 6a), one strain gauge placed on the concrete surface (C1 in Fig. 6a) and three internal gauges placed on longitudinal reinforcement (S1, S6 and S7 in Fig. 6b). In addition, a 3x3 mesh of discs was glued on the beam's lateral surface to measure deformations with a demountable mechanical strain gauge (DEMEC). Measurements with DEMEC were taken twice weekly.

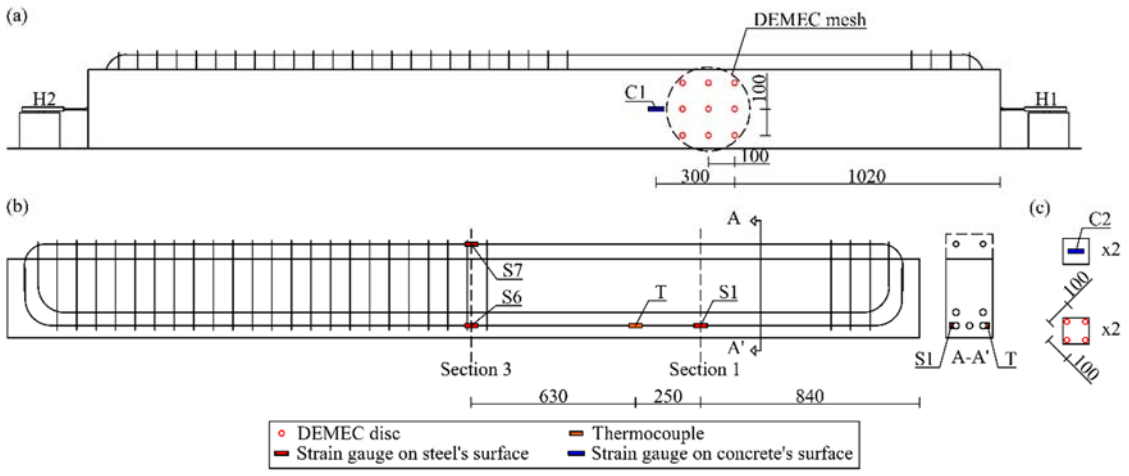

Fig. 6. Instrumentation for the shrinkage measurement of a beam of series DO: (a) external instrumentation; (b) internal instrumentation; (c) instrumentation of a concrete cube (dimensions in mm).

To measure internal temperature, a thermocouple was placed inside each beam (T in Fig. 6b). Ambient temperature and humidity were constantly measured.

Two concrete cubes (100x100x100 mm) were fabricated while casting the beam's concrete to measure free shrinkage by means of two strain gauges and two 2x2 meshes of DEMEC discs on each cube (see Fig. 6c).

2.6. Test setup and procedure

A steel-loading frame with a 1200 kN hydraulic actuator was used to perform the shear tests (Fig. 7a). Beams were laid on two supports (250 mm width) equipped with a steel balls bed each to eliminate the horizontal reaction, as shown in Fig. 7c. Both bearing points allowed rotations on the frame's plane. A steel beam was designed to divide the load of the actuator into two point loads (Fig. 7b). It was connected to a hinge joint for the load to remain vertical all the time. This steel beam transmitted load to specimens through 200x200x30 mm steel load plates. Load was applied with the displacement control (0.02 mm/s).

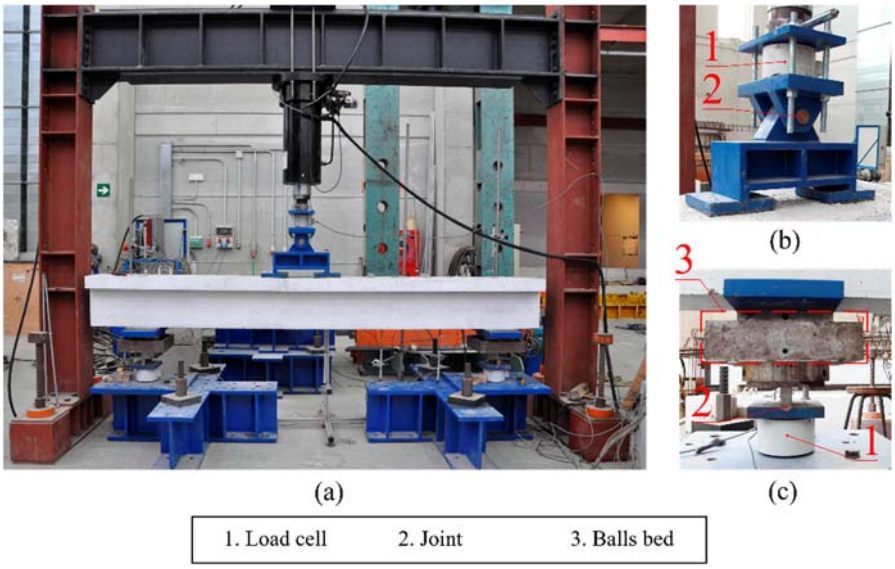

Fig. 7. Experimental setup and testing frame: (a) general view; (b) two-point loading system; (c) bearing points system.

3. Test results and discussion

3.1. Shear-deflection relation

The shear at the non-reinforced span (principal span) and the deflection below the point load closest to that span (LVDT V4 in Fig. 5a) were measured. Fig. 8 shows the shear-deflection relation measured in all the test specimens, except specimens NOP3B1 and NOP3C1 due to a failure of the LVDTs during tests. As seen in Fig. 8b-d, composite beams' curves are presented together with their homologous monolithic beams' curves. In order to facilitate the reading of the graphs, series DO beams are represented separately in Fig. 8e. Most of the beams tested in this test programme, both monolithic and composite, underwent two local maximums in shear, as seen in the graphs. The first local maximum corresponded to the critical shear crack appearing.

After the load drop, the load-carrying capacity of most tested specimens continued to increase, which gave a second local maximum in the shear-deflection relation. In some cases, this second maximum was higher than the first one.

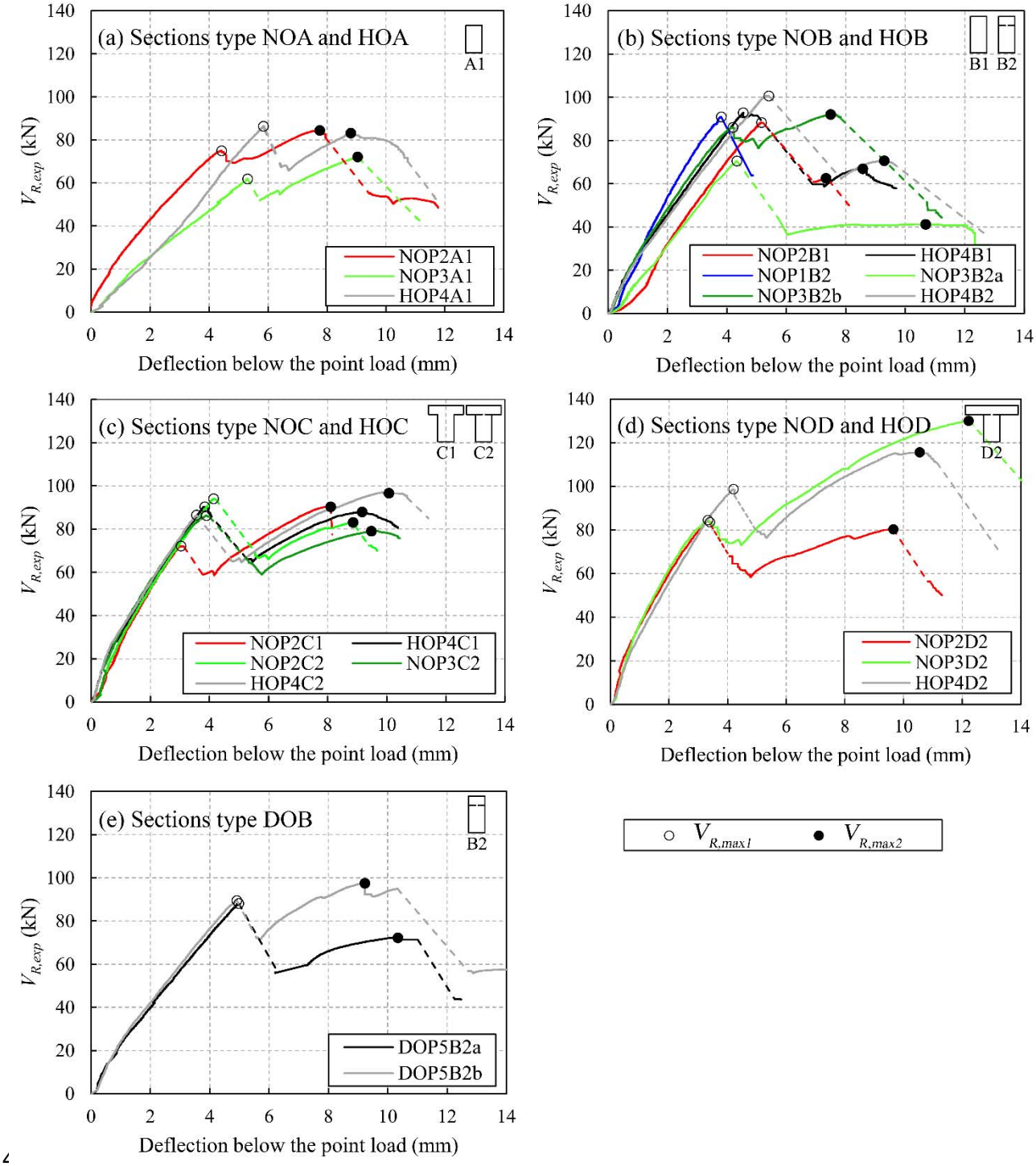

Fig. 8. Shear-deflection relation of all the test specimens: (a) sections type A; (b) sections type B from series NO and HO; (c) sections type C; (d) sections type D; (e) sections type B from series DO. (Specimens NOP3B1 and NOP3C1 not included: failure of LVDTs).

3.2. Shear strength

3.2.1. Vertical shear strength

Table 2 shows the shear values for the first and second local maximums ($V_{R,max1}$ and $V_{R,max2}$) of the shear-deflection curves.

All specimens failed in shear. The maximum strains measured along the tension longitudinal reinforcement (1.4‰) were far from the yield strain (2.8‰).

3.2.2. Interface horizontal shear stresses

The average horizontal shear stress at the interface $\tau_{R,exp}$ concurrent with $V_{R,max1}$ was obtained experimentally from the strains provided by the gauges located on both the concrete surface and the longitudinal reinforcement at Sections 1, 2 and 3 (see Fig. 5). For each section, a plane distribution of strains was defined by the compression strain on the concrete surface (or the strain at the compression longitudinal reinforcement in Section 3) and the strain on the tension reinforcement. The three strains measured on top of the concrete slabs of the specimens with flanges were similar in all the T-shaped specimens; that is, no evidence for shear lag was detected until shear's first local maximum was reached. Nevertheless, only the strains measured by the central strain gauges were used in the obtaining of the strains plane (gauges C2 and C5 in Fig. 5b). The strains plane was turned into a distribution of stresses using the Sargin's concrete constitutive curve and the steel constitutive curve described in EC2 [11]. By integrating only the compression stresses above the interface, or above the neutral axis if it was located over the interface, and including the stresses at compression longitudinal reinforcement, compression force C was obtained for all three instrumented sections. Tension stresses of concrete below the neutral axis were neglected. The horizontal shear stress at the interface between the beam's and the slab's concretes of a stretch i of the composite beam ($\tau_{R,exp,i}$) was calculated by dividing the difference of the compression forces between two consecutive cross-sections by distance x between both sections and beam width b (1). Table 2 shows the average value of the horizontal shear stress of the three stretches ($\tau_{R,exp}$) for those composite specimens in which horizontal cracking at the interface occurred at $V_{R,max1}$ (see the "Cracking mode" column at Table 2).

$$\tau_{R,exp,i} = \frac{C_i - C_{i-1}}{x_{i,i-1} \cdot b} \quad (1)$$

The method to calculate the horizontal shear stress is only valid if there is no slip between concretes at the interface. This slip was controlled by the horizontal LVDTs

described in Fig. 5. It was verified that the slips recorded by horizontal LVDTs were almost negligible in all the specimens until $V_{R,max1}$ was reached. After the formation of the critical shear crack, the interface between concretes was usually cracked, what caused a discontinuity in the strains plane. Thus the calculation of horizontal shear by this method was not possible after $V_{R,max1}$.

3.3. Crack pattern observations

Fig. 9 shows the crack patterns of the tested beams grouped according to section type. In this figure, the cracks observed until shear's first local maximum $V_{R,max1}$ are represented by a thin black line; those cracks that appeared immediately after $V_{R,max1}$ are denoted by a thick black line; orange depicts the cracks observed until shear's second local maximum $V_{R,max2}$; blue indicates the cracks that appeared after $V_{R,max2}$ with definitive specimen collapse.

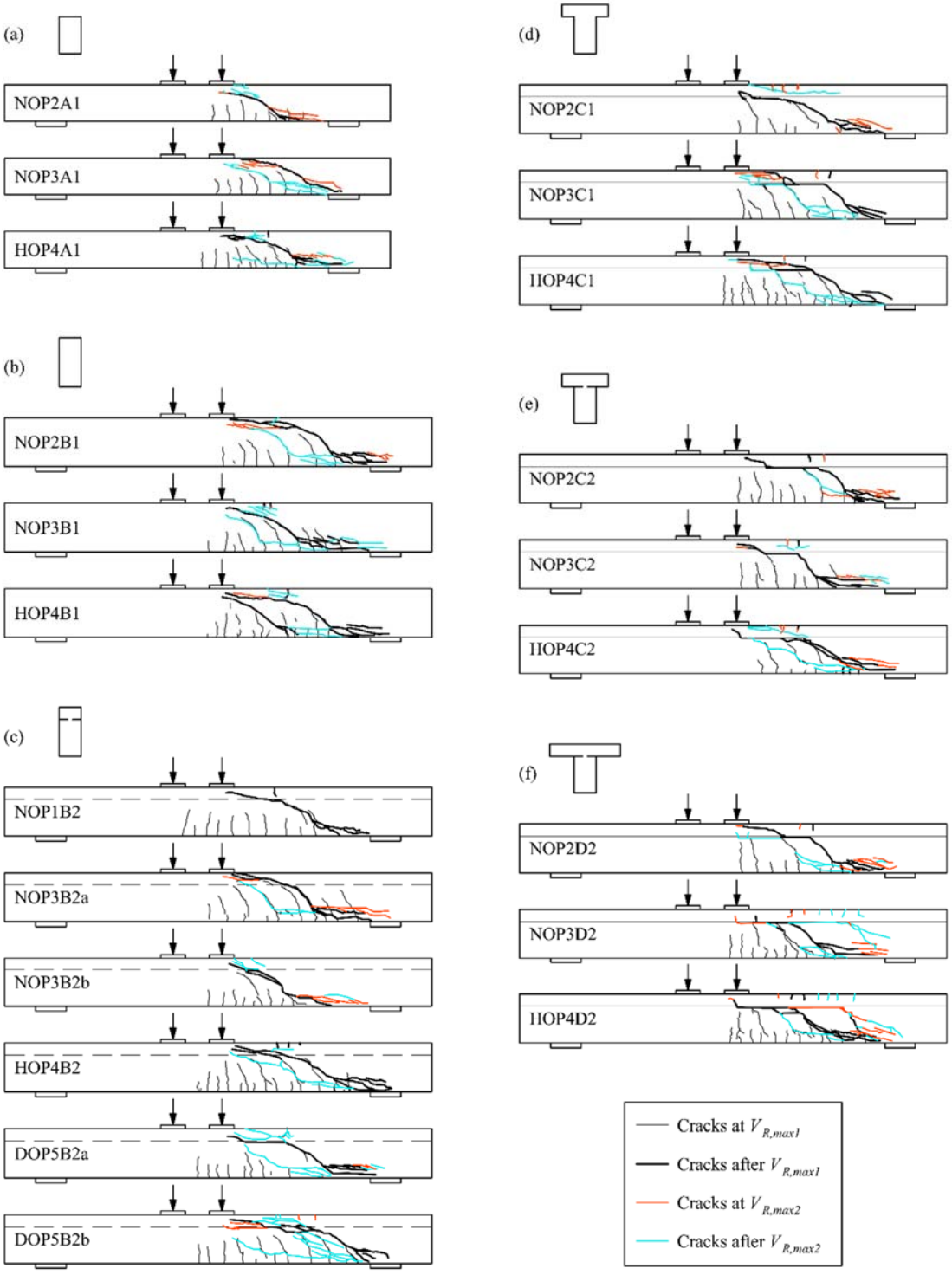

Fig. 9. Crack patterns of the test specimens in different test stages grouped according to section type: (a) A1; (b) B1; (c) B2; (d) C1; (e) C2; (f) D2.

3.3.1. Cracking at $V_{R,max1}$

The first cracks noted in all the specimens, regardless of their cross-sectional shape, were bending cracks, which rose from the bottom of the beam (see A in Fig. 10a). As load increased, some of these vertical cracks extended to the neutral axis (B in Fig. 10a) by roughly following a quasi-vertical direction, just as Fernández *et al*. stated [24].

These cracks became flatter on a second branch of the crack above the neutral axis [1] to thus form diagonal shear cracks (branch C in Fig. 10a). This behaviour occurred similarly for the rectangular and T-shaped beams until the crack reached the plane where the cross-sectional width increased. When shear's first local maximum was reached, the specimens' crack pattern was similar to that shown in Fig. 10a.

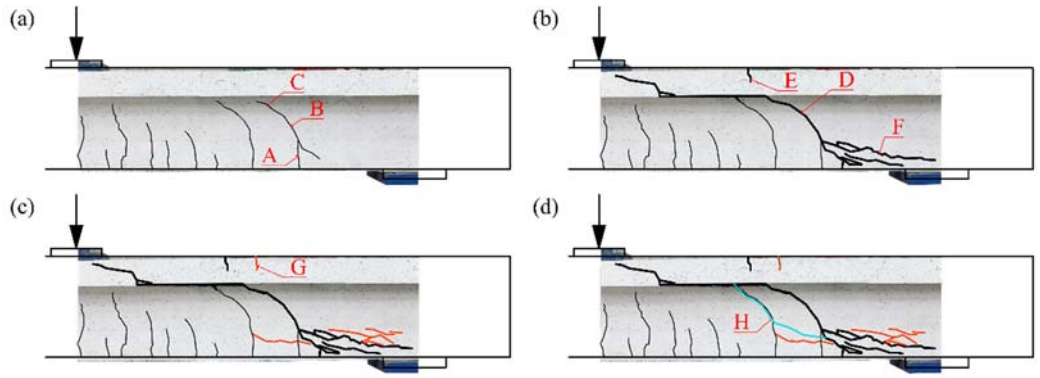

Fig. 10. Example of crack pattern of specimen NOP2C2 at different load stages: (a) at $V_{R,max1}$; (b) after $V_{R,max1}$; (c) at $V_{R,max2}$; (d) after $V_{R,max2}$.

3.3.2. Cracking after $V_{R,max1}$

Once shear's first local maximum had been reached, load drop took place due to entire diagonal critical crack tip development (D in Fig. 10b). The shape of the critical crack in the compression chord showed differences from one beam to another.

In monolithic beams with rectangular cross-sections, two different behaviours were observed in critical crack tip development. In some specimens, the critical crack crossed the beam depth and left a very tight compression chord, or even crossed it completely until the extreme compression fibre of the cross-section was reached (described by Zararis as the splitting of concrete in the compression chord [25]). An example of this crack pattern was observed in specimen NOP3A1 (Fig. 9a). In other specimens, the critical crack finished well below the load plate, and left uncracked a considerable depth of the compression chord, as seen in specimen NOP2A1 (Fig. 9a). In the rectangular composite beams, an interface existed between concretes that could deviate the direction of the critical crack by forcing it to develop through the interface before accessing the slab (see Fig. 9c and the "Cracking mode" column of Table 2).

In the T-shaped monolithic beams, a discontinuity in the cross-section width modified the direction of the critical crack by forcing it to develop along the plane in which the section width changed. This behaviour has been already observed in previous research works with T-shaped monolithic beams without web reinforcement [1], where the two following crack pattern types were noted. Firstly, the crack pattern with a delamination

crack [16], in which the critical crack developed horizontally when reaching the plane in which the beam width changed and developed along it over a long stretch before accessing the T-shaped beam head. For example, specimen NOP2C1 displayed this crack pattern (Fig. 9d). Secondly, the crack pattern with a diagonal crack at the head [15,16], in which the critical crack at the web crossed the plane in which beam width changed and continued as an inclined crack in the head, as seen in specimen HOP4C1 (Fig. 9d). In both crack patterns, the appearance of vertical cracks starting from the starting on top of the head was observed, which indicates head bending (E in Fig. 10b). In the T-shaped composite beams, the interface forced the critical crack to develop along the plane in which the section width changed at a longer distance (Fig. 9e-f).

In all the specimens, the formation of different longitudinal cracks was observed at the level of the tension longitudinal reinforcement after the entire critical shear crack had developed. These cracks developed from the end of the critical crack to the support of the element (see F at Fig. 10b).

3.3.3. Cracking at $V_{R,max2}$

Critical shear crack development did not lead to the collapse of all the specimens. Some beams underwent increased load, with a second local maximum in shear. The gradual formation of new cracks took place (Fig. 10c).

Having reached shear's second local maximum, almost all the beams presented new longitudinal cracks at the tension longitudinal reinforcement level and the length of the existent ones grew (see Fig. 9). In some specimens, the length of the diagonal critical crack tip increased.

In all the T-shaped beams, new bending vertical cracks appeared at the top of the slab (G in Fig. 10c). This was also observed in the rectangular composite beams in which the interface substantially modified the direction of the critical shear crack, as seen in specimen DOP5B2b (Fig. 9c).

In the beams whose shear's second local maximum was very high, such as specimens NOP3D2 and HOP4D2 (Fig. 8d), a new crack developed along the interface in the direction towards the support (Fig. 9f).

3.3.4. Cracking after $V_{R,max2}$

After reaching the shear's second local maximum, specimens collapsed. In many tested beams, an already existent diagonal shear crack opened, which differed from the critical crack and was closer to the point load than the latter (H in Fig. 10d), and multiple longitudinal cracks formed at the tension longitudinal reinforcement level. By

way of example, see beam NOP2B1 in (Fig. 9b). In other specimens, the crushing of concrete at the compression chord was observed. This happened in those beams in which the compression chord had remained almost intact after critical shear crack had formed (e.g. beams NOP2A1, HOP4A1 and NOP3B2b). In other specimens like NOP2C1 and HOP4C2, diagonal slab cracking occurred. A combination of these crack patterns was also observed in some beams; that is, the opening of another diagonal crack and the crushing of concrete in the compression chord, as seen in beams NOP3B1 and DOP5B2a. All these crack patterns are observed at Fig. 9.

Specimens NOP3D2 and HOP4D2 collapsed with the opening of the crack that appeared at the interface in the direction towards the support (see Fig. 9f).

3.4. Failure modes

The potential shear-carrying mechanisms that can be run to transfer shear force in the beams without stirrups were described by Fernández Ruiz, Muttoni and Sagaseta [24,26] among others. By considering the crack pattern observed in the beams herein tested, three phases were identified depending on the main shear-carrying mechanisms that resisted shear force: phase 1, until $V_{R,max1}$ was reached; phase 2, between $V_{R,max1}$ and $V_{R,max2}$; phase 3, after $V_{R,max2}$. Fig. 11 shows the three schematic strut-and-tie representations associated with these three phases.

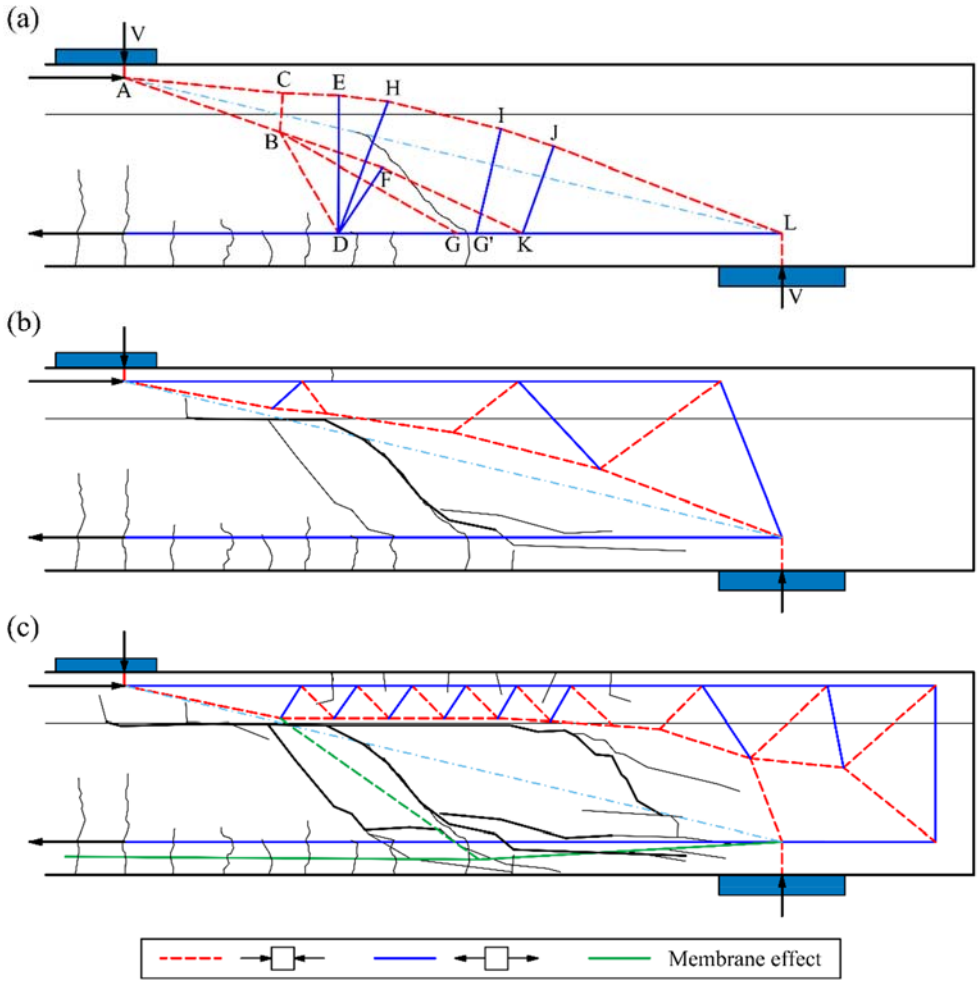

Fig. 11. Strut-and tie models of the shear transfer mechanisms observed, drawn on specimen NOP3D2: (a) development of diagonal cracks; (b) after critical shear crack formation; (c) collapse.

3.4.1. First phase: development of diagonal cracks

A first phase was observed until shear's first local maximum was reached, when the crack pattern was like that of specimen NOP3D2 shown in Fig. 11a, with a shear-deflection relation depicted in Fig. 8d.

Fig. 11a shows the strut-and-tie model that explains the load paths in this phase. A portion of shear force was transferred across the critical shear crack, mainly by aggregate interlock (strut FK), residual tensile stresses (tie DH) and dowel action (G-G'). The remaining shear force was transferred by the inclination of the compression strut (strut EH) above the critical shear crack tip.

The behaviour of all the tested specimens in this first phase was similar, regardless of them having a rectangular cross-section or a T-shaped section.

In this phase, the strain gauges located on top of beams showed compression strain. Immediately before the shear's first local maximum was reached, these gauges showed a slight compression strain reduction at the same time as the new diagonal

cracks appeared on the beam's web. This indicates a change towards other shear-carrying mechanisms.

3.4.2. Second phase: after critical shear crack formation

After reaching shear's first local maximum, the critical shear crack extended towards the applied load (Fig. 11b) and its width increased. A major load drop was recorded. Critical shear crack development disabled the cantilever action of the "tooth" (strut BD and tie DE in Fig. 11a) and the increasing crack width reduced the residual tension stress (tie DH in Fig. 11a), which made these shear-carrying mechanisms negligible.

In the T-shaped monolithic beams, the critical shear crack developed along the horizontal plane connecting the web and head of the beam (see Fig. 9d). In the rectangular composite beams, the interface between concretes could become a weak plane and, consequently, deviate crack development along that plane (e.g. in specimens NOP3B2b and DOP5B2a shown in Fig. 9c). In the T-shaped composite beams, the interface between concretes always deviated the critical crack direction (see Fig. 10b and Fig. 11b).

The increase in the critical crack width reduced the aggregate-interlock action, but increased the dowel action of the tension longitudinal reinforcement. However, the potential dowel action increment was truncated by the appearance of the longitudinal cracks at this longitudinal reinforcement level (Fig. 11b). Furthermore, the aggregate interlock and dowel actions reduced as new cracks (Fig. 11b) appeared in the tension zone above the shear critical crack (concrete ties G'I and KJ in Fig. 11a).

In this second phase, vertical cracks starting from the top of the slab appeared and the strain gauges placed on the upper side of the slab recorded tensile strains, which indicated the existence of tension stresses on the element's upper side. These observations evidenced the existence of an upper strut-and-tie system (Fig. 11b), which made the arching action over the critical shear crack possible. As Swamy *et al*. observed [16], specimens acted as a tied arch. This mechanism allowed shear force to increase until the shear's second local maximum $V_{R,max2}$ was reached.

3.4.3. Third phase: collapse

This phase is identified as specimens' failure after reaching the shear's second local maximum. Different behaviours were observed in this phase depending on the critical shear crack shape. Nonetheless, they can all be described by loss of the shear transfer mechanisms' capacity due to the arching action, with a clear loss of dowel action.

However, the great deflection of the longitudinal tie allowed a membrane effect to resist a portion of shear force (Fig. 11c).

The specimens' shear resistance capacity in this phase was governed mainly by the capacity of the arching action, which depended on the degradation level of the compression chord. In some specimens, the critical shear crack caused the splitting of concrete in the compression chord: it crossed almost its entire depth or narrowed it. This happened, for example, in specimens NOP2B1 and NOP2D2 (Fig. 9). In such cases, the arching action did not allow high shear's second local maximum values to be obtained.

Conversely in other specimens, load could flow over the critical shear crack in the direction to the support. The collapse of these beams was due to the crushing (i.e. DOP5B2b) or splitting (i.e. HOP4C2) of the concrete of the compression chord after major aching action took place thanks to the large enough depth of the compression chord that left the critical shear crack. These beams showed high over-strengths at shear's second local maximum. This behaviour was observed in, for example, specimens NOP2A1 and NOP2C1 (Fig. 9).

Specimens NOP3D2 and HOP4D2 had the highest over-strengths of the tested beams (Fig. 8d). In these cases, the compression chord was almost intact and a crack developed along the interface in the direction to the support. This effect forced the elbow-shaped strut to move towards the support, and to occupy a position at which it was unable to resist the existing shear force at the span. This led these elements to fail (see Fig. 11c).

As seen above, the existence, or not, of a shear's second local maximum greater than the shear's first local maximum in the beams of this experimental programme depended on: the critical shear crack shape, mainly at the compression chord; the presence of an interface between concretes; the existence of a geometrical discontinuity at the section width. However, not all the specimens with the same cross-section characteristics developed a second local maximum greater than the first one. Consequently, as no behaviour pattern could be defined, it was unsafe to take the absolute maximum as the element's shear strength. This measure was also adopted by Kim *et al.* in those specimens presenting an over-strength after diagonal tension cracking [2].

In the present study, in order to verify the design models, and based on structural safety criteria, specimens' shear strength was defined as the first shear's local maximum.

3.5. Influence of test parameters on shear strength

3.5.1. Contribution of a cast-in-place concrete slab

To study the contribution to shear strength of the cast-in-place concrete slab on top of the beams, the elements with section type A1 were compared to those with section type B2. This comparison was made by fabrication batches to avoid the influence of concrete strength variable. In Fig. 12, the experimental shear strength results are classified by section type and distinguishing the beams according to the fabrication batches.

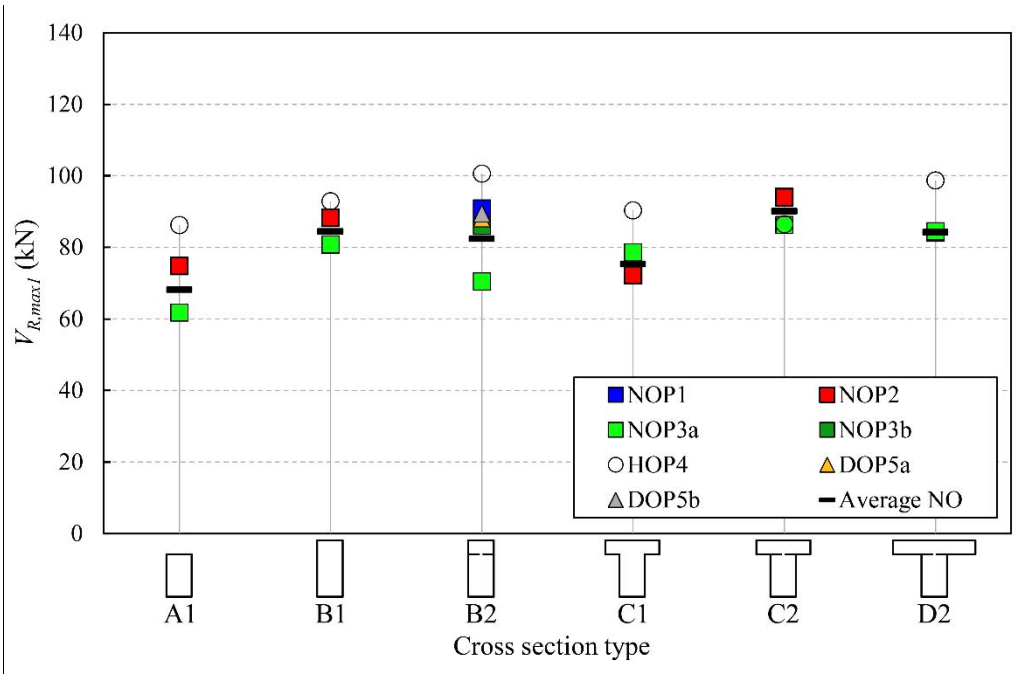

Fig. 12. Experimental shear strength of all the tested specimens corresponding to shear's first local maximum.

The shear strength of the B2 beams was, on average, 23% higher than that of the A1 beams of the same batch. This result was similar to that of the B1 beams compared to the A1 beams (19%). This increase in both cases was less than that of their respective effective depths (33%). Consequently, the slab did not increase the shear strength of the element in the same quantity as the effective depth increased. This minor shear strength increment in monolithic beams can be explained exclusively by the size effect, as the other parameters were identical. Since B1 and B2 beams' shear strengths were similar, the size effect could be also the main cause of this minor increment of the shear strengths of the B2 composite beams with respect to the A1 beams and not the weakness of the bond on the interface plane between concretes.

As Halicka pointed out [14], if the shear force that initiates interface cracking is lower than the shear force that leads to diagonal cracks appearing, the delamination of the

interface and thus, the horizontal shear failure, will take place prior to shear failure. As specimens were designed to avoid horizontal shear failure (Rueda *et al.* [19]), the cast-in-place concrete slab had the same effect as adding depth to the shear area, although interface cracking occurred.

3.5.2. Existence of an interface between concretes

The influence of an interface between concretes in specimens' shear strength was studied by comparing the behaviour of the B1 beams with the B2 beams of the same fabrication batch, and the C1 beams with the C2 beams of the same batch.

The B2 beams were expected to have intermediate shear strength between those of beams A1 and B1 because of the weakness of the interface between both concretes. However on average, the shear strength of beams B1 and B2 was similar (Fig. 12). In particular, specimens NOP3B2b and HOP4B2 had higher shear strengths than specimens NOP3B1 and HOP4B1, respectively. On the contrary, beam NOP3B2a presented lower shear strength than beam NOP3B1. Regarding the T-shaped beams, the specimens made of two concretes, C2, had a slightly higher shear strength than monolithic beams C1 when the average values of $V_{R,max1}$ for sections C1 and C2 were compared. However, this was not a regular behaviour. In particular, this over-strength was observed in the beams of batches NOP2 and NOP3, whereas a slightly decreased strength was noted in batch HOP4 (Fig. 12).

In the rectangular composite beams, the over-strength of the composite specimens was associated with the modification of the critical shear crack path, which spread along the interface plane because of its weakness. This modification changed the contribution of shear-transfer mechanisms and, as a result, shear resistance capacity increased. However, specimens NOP3B2a and NOP3B2b were assumedly identical, but had different crack patterns (Fig. 9), which evidences the uncertainty of the critical shear crack path shape.

In the T-shaped beams, the critical shear crack path always deviated due to the geometrical discontinuity in section width. In the composite T-shaped beams, the crack spread along the interface over a longer length.

It can be generally concluded that if a portion of the critical shear crack path developed along the interface, the composite beam had a higher shear strength than the monolithic beam. This could be due to the greater compression chord depth as the existence of an interface postponed the crack entering the slab, what left a wider concrete chord in both the rectangular and T-shaped beams.

3.5.3. Flange width

In order to study the influence of flange width on shear strength, the beams with section type B were compared to their homologous beams with sections C and D. From these comparisons, the following findings were drawn:

a) The flanges of the T-shaped monolithic and composite beams with section type C did not entail any increased shear strength compared to their homologous rectangular beams, neither when comparing shear's first local maximum nor its second one (see Table 2).
b) Shear's first local maximums of beams type D2 were comparable to those of sections B2 and C2 (Fig. 12). However, they showed higher shear's second local maximums because the critical shear crack path allowed a considerable arching action mechanism to develop. Thus specimen NOP3D2 showed an over-strength higher than 40% compared to sections B2 and C2 of the same batch, and specimen HOP4D2 displayed an over-strength over 15%.
c) Regarding crack patterns, a great similarity was observed between the beams with section types C2 and D2 (Fig. 9). When comparing fabrication batches, the critical crack of both beams had the same inclination and position in the principal span, regardless of flange width. The only difference between them laid in the critical crack developing in the compression chord: in some beams, it completely crossed it, but did not in other beams, which allowed the subsequent arching action mechanism to develop.

In view of the observed behaviours, it was verified that shear's first local maximum, which corresponded to diagonal beam cracking, was governed principally by the shear transfer actions that occurred at the beam's web: aggregate-interlock action and dowel action. The compression chord-related actions were not so relevant in this stage. Hence the rectangular and the T-shaped beams had similar shear strength upon the first local maximum. Consistently with Kani's predictions [17], high tension longitudinal reinforcement ratio ρ_l brought about a marked increase in dowel action, as well as increased aggregate-interlock action due to a crack widths reduction. This could imply a reduction in the contribution of flanges to shear strength, as Ayensa *et al*. observed [27].

At collapse, behaviour was almost entirely governed by the arching action (cantilever mechanism). The specimens in this experimental programme showed that the development, or not, of an over-strength thanks to flanges depended on how the critical shear crack altered the compression force path, as explained in Section 3.4 of this

paper. For example, after critical shear crack formation, the strength of specimen NOP2C1 could increase, but HOP4C1 could not, existing clear differences in the shape of their shear critical cracks (Fig. 9). Swamy and Qureshi [28] also observed the possibility of having a second stage in the shear strength of the T-shaped beams that may, or may not surpass, that at shear cracking.

Different results are found in the literature about the comparison of the shear strengths between the rectangular and T-shaped beams without web reinforcement. Authors like Placas and Swamy *et al.* [15,16] observed the same failure type and at the same load of T-shaped beams and their homologous rectangular beams in beams with a similar shear span-effective depth ratio to that in this programme. In Placas [15], beams with a/d = 3.4 and ρ_l = 1.46% were tested, while in Swamy *et al.* [16], beams with a/d = 4.0 and ρ_l = 1.70% for rectangular beams or ρ_l = 2.67% for T-shaped beams were used. Other authors like Kotsovos [29] obtained higher strengths in T-shaped beams, apparently in a second local maximum after diagonal cracking in beams with a/d = 3.3 and ρ_l = 5.20%.

In this experimental programme, the T-shaped beams that had an over-strength in shear capacity showed that the flange width in beam type C (once the slab depth) was not wide enough to develop a considerable over-strength by arching action, as their shear strength was similar to that one in the rectangular beams. However, flange width in beam type D (twice the slab depth) was wide enough. It should be highlighted that this over-strength was possible thanks to the transverse reinforcement provided in the slab, which allowed shear transfer through flanges. Without this mesh, failures caused by the shear between web and flanges would have been observed [17].

3.5.4. Concrete strength

In the composite beams, the series HO specimens were compared to their series NO homologous specimen to analyse the influence on shear strength of using different compressive concrete strengths for both beam and slab.

In most cases, the specimens with a high-strength concrete (HSC) in the beam displayed slightly more shear strength (4% on average) than the beams made of normal-strength concrete (NSC), as seen in Fig. 12. The monolithic beams made of HSC had higher strength than the beams made of NSC. In these cases, as HSC was present over the entire concrete section, it was not possible to conclude whether this higher strength was due to the presence of HSC in the beam's web or at the compression chord. With the composite beams, the HO beams also showed higher strength than those of series NO (except HOP4C2, with a similar strength to NOP2C2

and NOP3C2, what could only be explained by the variability associated to concrete's shear behaviour uncertainties). As NSC was present in the slabs of both series, it was deduced that, for the specimens of this experimental programme, diagonal tension cracking was governed mostly by the web's concrete strength. Hence the greater the web's concrete strength, the higher the shear at which the diagonal cracking occurs.

Shear's second local maximum was analysed by studying the beams in which shear's second local maximum was higher than the first one. When normalising specimens' shear strength by the square root of the compressive strength of the slab's concrete, the beams with the same cross-section type had the same ratio. The beams D2 were particularly remarkable, as the dispersion of shear's second local maximum was considerable. This result is shown in Fig. 13. It was deduced, therefore, that the arching action mechanism was governed mostly by the slab's concrete strength, as previous authors have stated [2]: shear capacity increases with the slab's concrete strength.

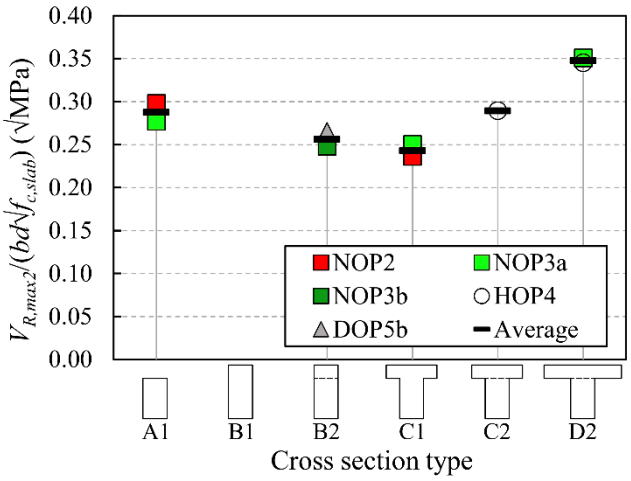

Fig. 13. Normalised shear strength of specimens in which shear's second local maximum was higher than shear's first local maximum.

3.5.5. Differential shrinkage

As explained in Section 2.3, the slab's concrete of the specimens in series DO was cast when the beam's shrinkage was considered stabilised. After approximately 70 testing days, the measurements taken by the instrumentation started to achieve an asymptotic behaviour in relation to time, after which time shrinkage was limited. This asymptote was reached at an average strain of concrete gauges of 0.7‰ and an average strain of internal steel gauges of 0.12‰. The ambient temperature and that measured by the internal thermocouples was around 26ºC throughout testing. The average ambient humidity was 64%.

The beams of series DO were compared to their homologous beams in series NO to study how the differential shrinkage between different aged concretes would influence shear strength.

In the series DO specimens, the interface between concretes clearly modified the direction of the critical crack by forcing it to propagate along the interface over a considerably long stretch (see Fig. 9c). In fact this behaviour allowed specimen DOP5B2b to display a subsequent over-strength by the arching action mechanism. On the contrary in the beams of series NO, the interface deviated the critical shear crack over a short stretch (specimens NOP1B2 and NOP3B2b) or it even did not modified it (specimen NOP3B2a). This observed behaviour in the beams of series DO can be explained by the shrinkage stresses that generate when there is a difference in the shrinkage of the composite beam's concretes [18].

Regarding specimens' shear capacity, when shear's first local maximums were observed (see Fig. 12), the shear strength of series DO was similar to the shear strengths obtained in the beams B2 of series NO.

As a result of these observations, it was deduced that the use of different aged concretes at the beam and the slab modified the cracking pattern of the composite beams, but did not significantly change the vertical shear strength of the specimens. However, it is not possible to generalize this conclusion to other beam geometries and weather conditions. A more detailed experimental study should be conducted in that case.

4. Comparison of test results with existing code provisions

4.1. Vertical shear strength

Fig. 14 shows the relation between the experimental shear's first local maximum, and the shear strength predicted by design codes ($V_{R,max1}/V_{R,code}$) for the monolithic (A1, B1 and C1) and composite (B2, C2 and D2) specimens. The considered codes were EC2 [11] (Fig. 14a), ACI 318-19 [6] (Fig. 14b), and MC-10 [10] at its two approximation levels for the beams without web reinforcement: Level I (Fig. 14c) and Level II (Fig. 14d). The different codes' shear formulations are gathered in Table 4. The tested average values of the materials were used. In all cases, the partial safety factor for concrete γ_c and steel material properties γ_s was 1.0, and the used concrete section

width (*b*) was the web's width for all the cross-sectional shapes as codes disregard the contribution of flanges.

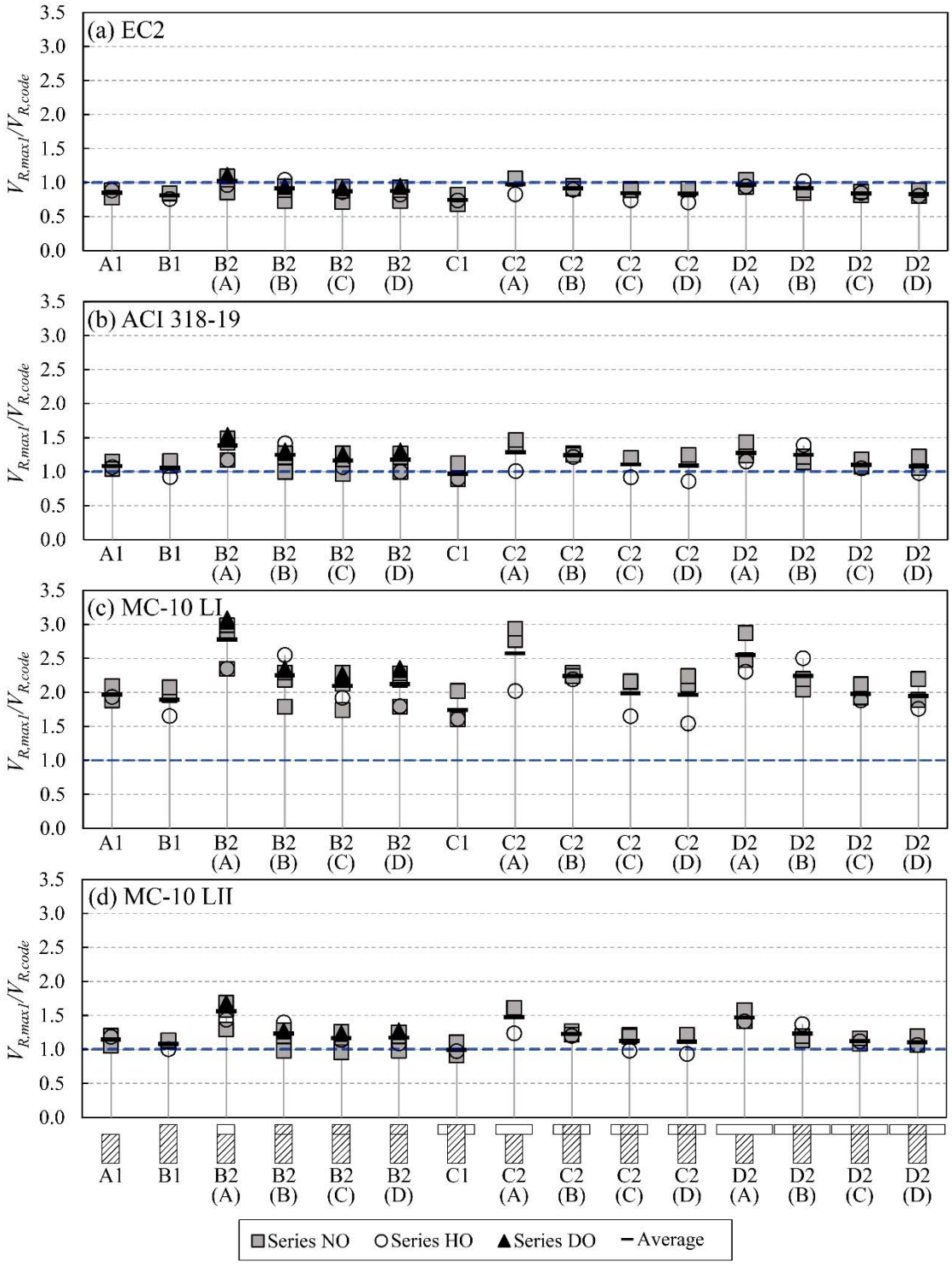

Fig. 14. Relation between the experimental shear strength and the predicted shear strength by design codes for all the tested specimens: (a) EC2 [11]*; (b) ACI 318-19* [6]*; (c) MC-10 Level I* [10]*; (d) MC-10 Level II* [10].

Table 4. Codes' shear capacity formulations for beams without web or interface reinforcement.

Code	Vertical shear strength equations (kN)	Horizontal shear strength equations (MPa)
EC2 [11]	$V_{R,code} = C_{R,c}k(100\rho_l f_c)^{1/3}bd10^3 \geq v_{min}bd10^3$ where $C_{R,c} = 0.18$; $k = 1 + \sqrt{\frac{200}{1000d}} \leq 2.0$; $v_{min} = 0.035k^{3/2}f_c^{1/2}$	$\tau_{R,code} = c_a f_{ct} + \mu\sigma_n \leq 0.5\nu f_c$ where $\nu = 0.6\left(1 - \frac{f_c}{250}\right)$ See c_a and μ values at section 6.2.5(2) [11]
ACI 318-19 [6]	$V_{R,code} = 664.3\lambda_s\lambda\rho_l^{1/3}\sqrt{f_c}bd \leq 415.2\lambda\sqrt{f_c}bd$ where $\lambda_s = \sqrt{\frac{2}{1+3.94d}} \leq 1.0$; λ=1.0 for normalweight concrete	$\tau_{R,code} = 0.55$
MC-10 Level I [10]	$V_{R,code} = k_v\sqrt{f_c}zb10^3$ (if $f_c \leq 70$ and $d_g \geq 0.010$) where $\sqrt{f_c} \leq 8$; $k_v = \frac{0.18}{1+1.25z}$	$\tau_{R,code} = c_a f_{ct} + \mu\sigma_n \leq 0.5\nu f_c$ where $\nu = 0.55\left(\frac{30}{f_c}\right)^{1/3} < 0.55$ See c_a and μ values at tables 7.3-1 and 7.3-2 [10]
MC-10 Level II [10]	$V_{R,code} = k_v\sqrt{f_c}zb10^3$ where $\sqrt{f_c} \leq 8$; $k_v = \frac{0.4}{1+1500\varepsilon_x}\frac{1.3}{1+k_{dg}z}$; $\varepsilon_x = \frac{1}{2E_s\rho_l bd}\left(\frac{M_{Ed}}{z} + V_{Ed}\right)$; $k_{dg} = 1$ (if $f_c \leq 70$ and $d_g \geq 0.016$); $k_{dg} = \frac{32}{16+1000d_g}$ (if $f_c \leq 70$ and $d_g < 0.016$); $k_{dg} = 2$ (if $f_c > 70$);	

All variables but f_c, f_{ct} and σ_n in SI units (f_c, f_{ct} and σ_n in MPa).

In all the specimens the horizontal shear limit state was experimentally verified because all the failures were brought about diagonal cracking. Therefore, according to the indications of EC2 and ACI 318-19 about composite beams' shear strength, it was possible to evaluate the composite beams as elements in which the slab's depth formed part of the shear strength area. Nonetheless, in this Section, the composite specimens' shear strength was calculated considering that only the beam contributed to resist shear (Case A), in order to compare this result with the entire composite member's shear strength. To calculate the composite specimen's shear strength, considering the contribution of the slab's depth, the two calculation methods that ACI 318-19 proposes for composite members where the specified concrete compressive strength, unit weight, or other properties of different elements vary were used: using the properties of the element that result in the most critical value of shear strength, in which case $f_{c,min}$ was used (Case B); or using the properties of the individual elements, in which case the weighted average of the concrete strengths of the beam and the slab $f_{c,wa}$ was used (Case C), as it was observed in Kim *et al.* [2]. Additionally, the entire composite specimen's effective depth and the compressive strength of the beam's concrete were used (Case D). The four cases were calculated with all the considered codes (EC2, ACI 318-19 and MC-10) for comparison (see Fig. 14).

Table 5 shows the following statistical indicators of the relation $V_{R,max1}/V_{R,code}$ calculated with each code for the 9 monolithic beams of this experimental programme: mean value, coefficient of variation CV (calculated as the ratio of the population standard deviation to the mean), minimum and maximum values, and number of unsafe results

of 9 beams. Table 6 shows the same statistical indicators for each code and for Cases A, B, C and D of the 12 composite specimens.

Table 5. Statistical indicators of the relation $V_{R,max1}/V_{R,code}$ for the 9 monolithic specimens.

Code	EC2	ACI 318-19	MC-10 LI	MC-10 LII
Mean	0.81	1.03	1.87	1.08
CV (%)	8.06	9.84	9.97	8.57
Minimum	0.69	0.89	1.60	0.91
Maximum	0.89	1.15	2.09	1.20
No.unsafe	9	3	0	2

Table 6. Statistical indicators of the relation $V_{R,max1}/V_{R,code}$ for the 12 composite specimens.

Code	EC2				ACI 318-19				MC-10 LI				MC-10 LII			
Case	A	B	C	D	A	B	C	D	A	B	C	D	A	B	C	D
Mean	1.00	0.92	0.86	0.86	1.33	1.25	1.13	1.13	2.67	2.25	2.04	2.04	1.52	1.23	1.15	1.15
CV (%)	9.04	8.40	7.81	9.04	12.67	8.49	9.94	12.67	12.67	8.49	9.94	12.67	9.67	8.45	8.07	9.52
Minimum	0.83	0.73	0.72	0.71	1.01	0.99	0.91	0.86	2.02	1.79	1.65	1.54	1.24	0.98	0.96	0.94
Maximum	1.11	1.04	0.94	0.95	1.54	1.41	1.27	1.31	3.09	2.55	2.29	2.36	1.69	1.40	1.26	1.28
No.unsafe	5	10	12	12	0	1	2	4	0	0	0	0	0	1	2	2

As seen in Table 5, ACI 318-19 and MC-10 LII gave quite accurate estimations of the monolithic elements' shear strength (mean values of 1.03 and 1.08, respectively). When comparing the results for monolithic and composite specimens (Table 5 and Table 6), the codes better estimated the shear strength of the monolithic beams; thus, the composite specimens' shear strength was underestimated by the codes' formulations using the four perspectives A, B, C and D (except for EC2, that gave, in most cases, unsafe results).

For the composite beams of series NO and DO, the models gave results that lay more on the safety side when only the beam was used to calculate shear strength (Case A) instead of using both the beam and slab (Cases B, C and D), as seen in Fig. 14. In the composite beams of series HO, Case B gave safer results than Cases A, C and D when codes EC2, ACI 318-19 and MC-10 LI were employed given the use of the lower f_c of the slab in the calculations. Cases C and D gave the same mean values for all the codes, but with a higher coefficient of variation in Case D.

EC2 gave a very unsafe shear strength estimation in the monolithic beams. In the composite specimens, only Case A gave a good estimation, although with several unsafe results (see Table 6). Thus, using the entire depth of the composite beam gave an unsafe estimation in Cases B, C and D. It should be noted that EC2 is currently

undergoing a revision process in which the shear strength formulation for members not requiring design shear reinforcement is particularly being revised.

ACI 318-19 well estimated the monolithic specimens' results with a low coefficient of variation (9.84%). For composite specimens, Case B gave a better estimation than Case A, with almost none unsafe results (1 beam). When using the $f_{c,wa}$ in the calculations (Case C) the estimation was even better (the mean value of $V_{R,max1}/V_{R,code}$ was 1.13) and still with few unsafe results (see Table 6). Case D, that is using the beam's f_c, gave the same mean value as Case C, but more scattered and with more unsafe results. This code showed the best approximation of the shear strengths to the actual ones, staying on the safety side.

MC-10 LI provided a very simple formulation, but gave very safe results for both monolithic and composite specimens. MC-10 LII fitted the results much better than LI. The monolithic beams' shear strength prediction by MC-10 LII was quite accurate. For composite specimens, Case C gave a good estimation with a low coefficient of variation (8.07%) and a few unsafe results (2 beams).

4.2. Horizontal shear strength

Table 7 shows the statistical indicators of the relation between the experimental horizontal shear stress at the interface $\tau_{R,exp}$ concurrent with $V_{R,max1}$ and the predicted horizontal shear stress by design codes $\tau_{R,code}$ for the composite beams of this experimental programme. Just the composite beams in which interface cracking took place at $V_{R,max1}$ were included in this analysis. Thus, beams NOP3B2a and HOP4B2 were excluded (see the "Cracking mode" column of Table 2). Specimen NOP3D2 was not included as the strain gauges for calculating the experimental horizontal shear stress failed. The used codes were: EC2 [11], ACI 318-19 [6] and MC-10 [10]. Their horizontal shear strength equations for interfaces without reinforcement crossing it are presented in Table 4. No unsafe results were obtained with any employed code.

Table 7. Statistical indicators of the relation $\tau_{R,exp}/\tau_{R,code}$ for the composite beams of this experimental programme with interface cracking (9 specimen. NOP3D2 not included: failure of strain gauges).

Code	EC2	ACI 318-19	MC-10
Mean	2.36	3.54	1.88
CV (%)	14.95	16.37	14.95
Minimum	1.81	2.70	1.45
Maximum	2.96	4.70	2.36

Codes EC2 and MC-10 have a similar formulation based on the Mohr-Coulomb failure criterion. This criterion considers an increase in horizontal shear strength provided by

the lowest expected compressive stress resulting from an eventual normal force acting on the interface (σ_n), normally applicable to confined elements (see Table 4). In this case, the normal stresses acting on the interface were neglected, staying on the safety side, although it was known that compression struts crossed the interface along the span. The existence of normal compressive stresses at the interface could increase the horizontal shear strength of the composite beams [2].

The ACI 318-19 formulation has an experimental basis which, for the beams without the minimum interface reinforcement defined by this code, limits the horizontal shear strength at the interface to 0.55 MPa.

In view of the results presented in Table 7, all the models gave a very safe result. When looking at the coefficient of variation, the three used codes presented a similar dispersion for the beams in this experimental programme. EC2 gave more restrictive results than MC-10 because its coefficient for adhesive bond c_a for very rough interfaces is lower. ACI 318-19 presented the greatest dispersion of the used codes: the experimental horizontal shear stresses obtained in the beams were between 1.48 and 2.59 MPa (see Table 2); that is, between 2.7- and 4.7-fold the ACI 318-19 prediction. Therefore, as Kim *et al.* already observed in their composite beams [2], ACI 318-19 underestimates the horizontal shear stress in beams with a very rough interface.

Consequently, it can be stated that codes underestimated the horizontal shear capacity of the concrete at the interface of the composite beams in this experimental programme. Therefore, the codes overestimate the required interface reinforcement to prevent horizontal shear failure. However, the interface's properties can be very different, although the same roughness is sought, as many variables take part: maximum aggregate size, concrete workability at casting, cleanliness of the interface, presence of laitance, concrete curing, differential shrinkage, etc. For this reason, it is justifiable that codes provide very safe expressions.

5. Summary and conclusions

The influence of a cast-in-place slab on the shear strength of composite reinforced concrete beams without web reinforcement was analysed in the present study. For this purpose, an experimental programme with 21 monolithic and composite beams subjected to shear was presented. The failure modes, the influence of an interface between different aged concretes, the cross-section shape, the strengths of the two

concretes and the effect of differential shrinkage were analysed. The main conclusions were the following:

1. Most of the tested beams in this test programme underwent two local maximums in shear. The first corresponded to critical shear crack formation. The second local maximum, sometimes higher than the first, was due to the deviation of the compression strut over the critical crack by the arching action mechanism.
2. The arching action's capacity depended on the degradation level of the compression chord after entire critical shear crack formation. In those specimens in which the critical shear crack caused the splitting of concrete in the compression chord, the arching action mechanism was unable to generally reach high second local maximums in shear strength. Conversely, the specimens in which the critical shear crack left intact a wide enough depth of the compression chord developed major arching action.
3. According to the analysed variables, no behaviour pattern was observed on the degradation of the compression chord after critical shear crack formation. Thus it was unsafe to take shear's absolute maximum as the element's shear strength.
4. For the beams in this experimental programme, it was demonstrated that, if the horizontal shear at the interface in the composite beams was verified, the cast-in-place concrete slab would increase the element's shear strength compared to the shear strength of only the beam as the slab was seen to add depth to the shear area.
5. In the composite rectangular beams, the interface between concretes was able to deviate the direction of the critical shear crack by forcing it to propagate along the interface before accessing the slab. In the T-shaped monolithic beams, the geometrical discontinuity in section width also deviated the direction of the critical crack along this weakness plane. In the T-shaped composite beams, the interface was a plane of weakness that always deviated the direction of the critical crack, normally by a longer length than in the T-shaped monolithic beams before entering the slab.
6. Both the rectangular beams and T-shaped beams had a similar shear's first local maximum as shear strength was governed by the shear transfer actions that occurred at the beam's web. Afterwards, some beams developed an over-strength at shear's second local maximum. It was observed that the flange width of beams type C (once the slab's depth) was not enough to develop a

high over-strength by the arching action, but did suffice in beams type D, where flange width was twice the slab's depth. These latter beams achieved the highest over-strengths.

7. In most cases, the specimens with HSC in the beam had slightly greater shear strength than the beams made of NSC in both the monolithic and composite beams. This proved that critical shear cracking was governed mostly by the web's concrete strength. Based on the experimental results, it was deduced that the arching action mechanism was governed mostly by the slab's concrete strength.
8. Differential shrinkage in series DO did not have a significant influence on the vertical shear capacity of the composite beams without shear reinforcement. It influenced, however, the observed cracking pattern, as the critical shear crack developed along the interface in a longer stretch than in the beams with a reduced differential shrinkage, what can be explained by the shrinkage stresses that generate when there is a difference in the shrinkage of the composite beam's concretes. However, this conclusion can not be generalized to other beam geometries and weather conditions, for which a more detailed study should be conducted.
9. As the compliance of the horizontal shear limit state in all the composite specimens was experimentally demonstrated, the shear strength of the composite beams without shear reinforcement was assessed with the codes' formulations in four ways: considering only the beam's shear strength and considering the entire composite beam's shear strength using $f_{c,min}$, the shear strength of the individual elements or the beam's f_c. Except for EC2 [11], which only provided a safe result when only the beam's shear strength was considered, the other codes showed a more accurate result when using the entire composite beam depth. Level I Approximation of the MC-10 [10] presented a simple but very safe formulation. Level II Approximation of the MC-10 [10] and ACI 318-19 [6] gave good results, especially when the sum of the individual elements' shear strengths was used. They were slightly conservative and gave only a few unsafe results. The four considered perspectives in calculating composite elements' shear strength, underestimated the actual shear strengths in comparison with the estimations made for monolithic beams, which were more accurate (except for EC2 [11] that provided very unsafe results for monolithic beams).
10. The codes underestimated the horizontal shear capacity at the interface of the composite beams without reinforcement crossing the interface. Therefore, the

required interface reinforcement to prevent horizontal shear failure is overestimated. The codes whose formulation is based on the Mohr-Coulomb failure criterion (EC2 [11] and MC-10 [10]) presented better results than ACI 318-19 [6], but were still far from the actual horizontal shear strength.

The experimental programme carried out in this research work contributes to increase the number of existent experimental tests of composite beams, which are necessary to improve current codes. However, in order to delve into the precast concrete construction field and the cast-in-place slab contribution to shear strength, further research in precast beams with web reinforcement and different cross-sectional shapes should be conducted.

Acknowledgements

This research has been supported by: the Spanish Ministry of Science and Innovation through Research Project BIA2015-64672-C4-4-R and RTI2018-099091-B-C21-AR; the Regional Government of Valencia through Project AICO/2018/250; the European Union with FEDER funds. The experimental programme was developed in the Laboratory of Concrete of the Institute of Concrete Science and Technology (ICITECH) of the Universitat Politècnica de València (UPV) with concrete supplied by Caplansa. The Spanish Ministry of Science and Innovation supported Lisbel Rueda through grant BES-2016-078010.

References

[1] Ribas González CR, Fernández Ruiz M. Influence of flanges on the shear-carrying capacity of reinforced concrete beams without web reinforcement. Struct Concr 2017. https://doi.org/10.1002/suco.201600172.

[2] Kim C-G, Park H-G, Hong G-H, Kang S-M. Shear Strength of Composite Beams with Dual Concrete Strengths. ACI Struct J 2016;113:263–74.

[3] Loov RE, Patnaik AK. Horizontal Shear Strength of Composite Concrete Beams With a Rough Interface. PCI J 1994;39:48–69.

[4] Kovach J, Naito C. Horizontal Shear Capacity of Composite Concrete Beams without Interface Ties. ATLSS Report No. 05-09: 2008.

[5] Fang Z, Jiang H, Liu A, Feng J, Chen Y. Horizontal Shear Behaviors of Normal Weight and Lightweight Concrete Composite T-Beams. Int J Concr Struct Mater

2018;12. https://doi.org/10.1186/s40069-018-0274-3.

[6] ACI Committee 318. Building code requirements for structural concrete (ACI 318-19); and commentary (ACI 318R-19). Farmington Hills: American Concrete Institute; 2019.

[7] Marí A, Cladera A, Bairán J, Oller E, Ribas C. Shear-flexural strength mechanical model for the design and assessment of reinforced concrete beams subjected to point or distributed loads. Front Struct Civ Eng 2014;8. https://doi.org/10.1007/s11709-014-0081-0.

[8] Avendaño AR, Bayrak O. Shear strength and behaviour of prestressed concrete beams. Technical Report: IAC-88-5DD1A003-3, Texas Department of Transportation: 2008.

[9] Shahawy MA, Batchelor B deV. Shear behavior of full-scale prestressed concrete girders: Comparison between AASHTO specifications and LRFD code. PCI J 1996;41.

[10] Fédération International du Béton (fib). Model Code 2010. Ernst & Sohn; 2012.

[11] CEN. EN 1992-1-1:2004. Eurocode 2: Design of concrete structures - Part 1-1: General rules and rules for buildings. 2004.

[12] Kim C-G, Park H-G, Hong G-H, Kang S-M, Lee H. Shear Strength of Concrete Composite Beams with Shear Reinforcements. ACI Struct J 2017;114:827–37.

[13] Halicka A, Jabłoński Ł. Shear failure mechanism of composite concrete T-shaped beams. Proc Inst Civ Eng Struct Build 2016;169:67–75.

[14] Halicka A. Influence new-to-old concrete interface qualities on the behaviour of support zones of composite concrete beams. Constr Build Mater 2011:4072–8.

[15] Placas A. Shear failure of reinforced concrete beams. Faculty of Engineering of the University of London. Imperial College of Science and Technology, 1969.

[16] Swamy R, Andriopoulos A, Adepegba D. Arch action and bond in concrete shear failures. J Struct Div 1970;96:1069–91.

[17] Kani MW, Mark W. Huggins, Rudi R. Wittkopp. Kani on shear in reinforced concrete. Toronto: University of Toronto, Dept. of Civil Engineering; 1979.

[18] Silfwerbrand J. Stresses and strains in composite concrete beams subjected to differential shrinkage. ACI Struct J 1997;94:347–53.

[19] Rueda-García L, Bonet Senach JL, Miguel Sosa PF. Influence of interface roughness and shear reinforcement ratio in vertical shear strength of composite concrete beams. In: ACHE, editor. VIII Congr. la Asoc. Española Ing. Estructural, ACHE, Santander: 2020.

[20] UNE-EN 12390-3:2020. Testing hardened concrete - Part 3: Compressive strength of test specimens. 2020.

[21] UNE-EN 12390-6:2010. Testing hardened concrete - Part 6: Tensile splitting strength of test specimens. 2010.

[22] UNE-EN 12390-13:2014. Testing hardened concrete - Part 13: Determination of secant modulus of elasticity in compression. 2014.

[23] UNE-EN ISO 6892-1:2017. Metallic materials - Tensile testing - Part 1: Method of test at room temperature. 2017.

[24] Fernández Ruiz M, Muttoni A, Sagaseta J. Shear strength of concrete members without transverse reinforcement: A mechanical approach to consistently account for size and strain effects. Eng Struct 2015;99:360–72. https://doi.org/10.1016/j.engstruct.2015.05.007.

[25] Zararis IP, Karaveziroglou MK, Zararis PD. Shear strength of reinforced concrete T-beams. ACI Struct J 2006;103:693–700.

[26] Muttoni A, Fernández Ruiz M. Shear strength of members without transverse reinforcement as function of critical shear crack width. ACI Struct J 2008;105.

[27] Ayensa A, Oller E, Beltrán B, Ibarz E, Marí A, Gracia L. Influence of the flanges width and thickness on the shear strength of reinforced concrete beams with T-shaped cross section. Eng Struct 2019;188:506–18. https://doi.org/10.1016/j.engstruct.2019.03.057.

[28] Swamy RN, Qureshi SA. An ultimate shear strength theory for reinforced concrete T-beams without web reinforcement. Matériaux Constr 1974;7:181–9. https://doi.org/10.1007/BF02473833.

[29] Kotsovos MD, Bobrowski J, Eibl J. Behaviour of reinforced concrete T-beams in shear. Struct Eng Part B R&D Q 1987;65 B:1–10.